Journal of Material Science & Engineering

Research Article   **Open Access**

High Temperature Oxidation Resistance of Ni$_{22}$Cr$_{11}$Al Bond Coat Produced by Spark Plasma Sintering as Thermal Barrier Coatings

Omoniyi FIS*, Olubambi PA and Sadiku ER

Department of Chemical, Metallurgical and Materials Engineering, Tshwane University of Technology, Pretoria, South Africa

Abstract

Thermal barrier coating (TBC) system is used in both aero engines and other gas turbines offer oxidation protection to super alloy substrate component. In the present work, it shows the ability of a new fabrication technique to develop rapidly new coating composition and microstructure. The compact powder were prepared by powder metallurgy method involving powder mixing and the bond coat was synthesized through the application of spark plasma sintering (SPS) at 1100°C, 1050°C and 1100°C to produce a fully dense 94%) Ni$_{22}$Cr$_{11}$Al bulk samples.

The influence of sintering temperature on hardness of Ni$_{22}$Cr$_{11}$Al done by micro vickers hardness tester was investigated. And oxidation test were carried out at 1100°C for 20 hr, 40 hr and 100 hr. The resulting coat was characterised with Optical microscopy, Scanning electron microscopy (SEM) and X-ray diffraction (XRD). Micro XRD analysis after the oxidation test revealed the formation of protective oxides and non-protective oxides.

Keywords: High temperature; Oxidation; Ni$_{22}$Cr$_{11}$Al; Spark plasma sintering; Thermal barrier coating

Introduction

In order to meet the challenging rising cost of high performance materials used for components operating at elevated temperature in aeroengines and other gas turbines, surface modification and techniques have attracted the attension of investigators globally [1,2]. Thermal barrier coatings are mostly used for this application. The TBCs are primarily made up of super alloy substrate, bond coat (BC) and YSZ topcoat, in which the bond coat layer is strongly linked to the oxidation behaviour of the TBC which affects its durability [3-5]. The bond coat is typically a platinum aluminide or NiAl based which provides oxidation and adhesion in the TBC System [6]. Application of TBC at elevated temperature gives rise to transfer of oxygen from the topcoat into the bond coat, so that an oxidized scale can be formed on the bond coat which is referred to as the thermally grown oxide (TGO) typically alfa-alumina [7,8].

However, this scale protects the super alloy components from further oxidation, the growth of TGO during thermal exposure leads to failure of the TBC System. This failure mechanism is generated at the TGO, the TGO/BC interface and the TBC. Studies shows that oxygen is transferred through ionic diffusion from the crystalline structure of ZrO$_2$ at the topcoat and penetration of gas through micro-cracks and porosities [9,10]. It has been proposed that these mechanism is facilitated mainly by the stress state arising from the residual compression in the TGO formed in service on bond coat which is the Al reservoir promoting α- alumina to form in preference to oxides [11-13]. In this study a Ni$_{22}$Cr$_{11}$Al bond coat were consolidated using spark plasma sintering technique and the high temperature oxidation resistance of the coating has been investigated.

Materials and Methods

Feed stock powder and characterization

Commercial starting powders for coating were Ni (flow master metal powder 28/0.5-3.0 micronparticle size 99.5% Ni), Cr (flow master metal powder<10 micron particle size, 99.2% Cr) and Al (flow master metal powder 99.7%) powders as bond coat. The three powders were mixed using the tubular shaker mixer T2F with the ball to powder ratio of 10:1 using stainless steel vial and five balls as milling media. Mixing speed of 72 rpm was chosen and a mixing time of 8 hr was allowed.

The Mixed powders were weighed according to Ni$_{22}$Cr$_{11}$Al molar composition as shown in Table 1. For the microstructures observations of the mixed powders, a small amount of the powders was mounted. The Cross section of the powders particles were prepared by conventional metallographic techniques. Microstructures and chemical composition of different phases in the powders were studied by employing Scanning electron microscope (SEM) with an energy dispersive spectrometer (EDS). The XRD analysis was done to identify the phases present in the samples in Bruker D$_2$. Advanced diffractometer using cobalt as anode material at 30 Kv and 10 MA. The powders were scanned at a step scan mode of 0.02.

Consolidation of the composites powders

In this work, the powders were consolidated by spark plasma sintering unit (H-HPD25-FCT Systeme GmbH Germany). The powders were loaded into a graphite die 20 mm in diameter and poured into packs of thickness between 3 to 8 mm in which 5 mm was aimed at. A Pressure of 30 MPa is applied to die through hydraulic rams fixed to a press. The current pulse of 3.3 ms fixed is generated by the power supply in which each pulse sequence contain 12 pulse was used. Temperature was measured by infra-red pyrometer to obtain a true value of temperature during consolidation. The densification process was carried out using a multistep heating method with heating rate of 100°C/min from room temperature to 1050°C. A holding time of 1 min

*Corresponding author: Omoniyi FIS, Department of Chemical, Metallurgical and Materials Engineering, Tshwane University of Technology, Pretoria, South Africa, Tel: 27123823598; E-mail: OmoniyiF@tut.ac.za, folorunsoomoniyi@gmail.com

Material	Ni	Cr	Al
NiCrAl	67%	22%	11%

Table 1: Chemical composition (in wt%) of $Ni_{22}Cr_{11}Al$ mixed feedstock powder.

at 600°C and 3.5 min at 1050°C.

Characterization of the sintered samples

The Sintered bulk surface were cleaned by grinding the surface using (Saphir 520 grinding machine made in Germany) with SiC P320 paper at speed 150 micron/min and a force 25 N for 30 min. Polished using both Aka-largan with dia max 9 micronmeter poly and Aka-napal with double 1 micronmeter poly to remove diffused carbon. The density of the sintered polished samples were performed by water displacement method (Archimedes principle process) using OHAUS density scale weighing balance of 0.001 mg accuracy. The density of the final sintered samples was 94% of the theoretical density.

Micro-hardness was measured using Vickers micro hardness tester (Future-Tech Corporation Tokyo, Japan) under loads of 25 gf for a dwell time of 10 secs. For the load five indents were made of which the average values were calculated. Fully dense SPsed samples were subjected to oxidation test in an electric furnace with an air atmosphere at 1100°C for 20, 40 and 100 hrs. Micro-XRD was carried out on the cross section of the sample after oxidation to determine the crystalline structure of oxide scales. SEM to investigate the microstructure and chemical composition.

Results and Discussion

Feedstock powder characterization

In Figure 1, XRD pattern for the mixed powders shows that there was mechanical activation of powders and also reactant phases. SEM micrographs of the mixed powder particles are represented in Figure 2, Mechanical mixing of the new material occurs, while there were still some regions which still consisted of one phase. EDS analysis showed that white areas are composed of aluminium and other areas encapsulating of Cr and Ni in softer Al particles which is visible extensively. Based on the XRD results of the mixed powders it can be expected that a reaction would occur during spark plasma sintering.

Sintering behaviours of the mixed powders during spark plasma sintering

Spark plasma sintering involves (relative piston travel as an indirect measure of densification and changes in the thickness of a sample die to movement of punches against the die with time is indicated by displacement [14-16]. The expansion or shrinkage is as a result of displacement towards the negative or positive direction [17].

The densification behaviour of the mixed powder was explained through the consideration of the shrinkage displacement and sintering time at different holding temperature during consolidation process [18,19].

$Ni_{22}C_{11}Al$ bulk samples were successfully densely sintered at 1050°C for holding time of 1 min at 600°C and finally 3 min under a pressure of 30 MPa. From Figures 3a-3c, the curve of displacement against temperature, it was observed that there was a preheating stage from room temperature to 585°C, thereafter shrinkage occurred at 970°C before thermal expansion of the dense sample at temperature greater or equal to 1050°C. This changes in displacement occurred due to sintering behaviour of the thermal expansion of the dense sample and the green body. And these behaviour could further be explained based
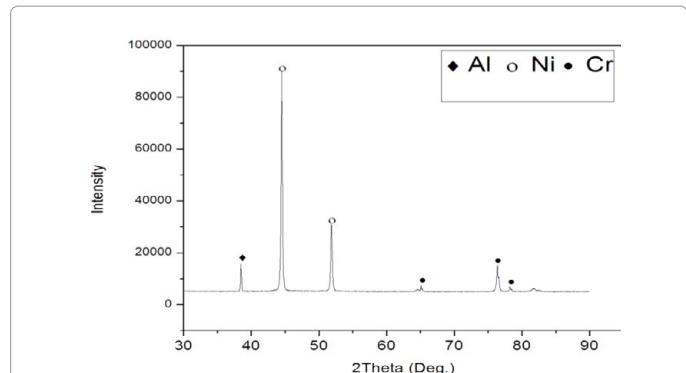

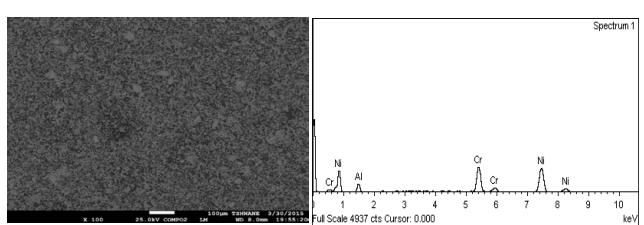**Figure 1:** XRD pattern of the mixed $Ni_{22}Cr_{11}Al$ powders.

Figure 2: SEM micrograph of the mixed $Ni_{22}Cr_{11}Al$ powders (Left), EDS analysis (Right).
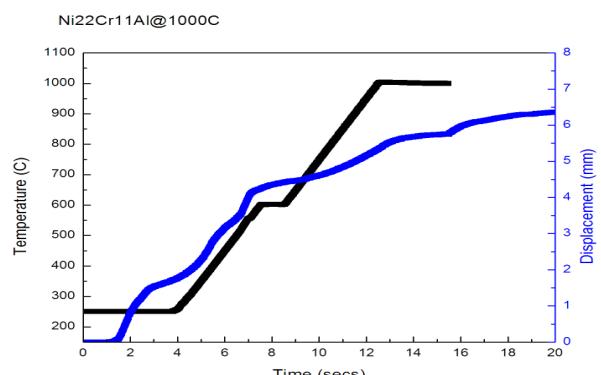

Figure 3a: The temperature and displacement curve in spark plasma sintering process at 1000°C.

on the fact that temperature was of great influence and important than the current during sintering process [20-23].

Characterization of microstructure, density and micro hardness

Figures 4 and 5 show the SEM images of sintered $Ni_{22}Cr_{11}Al$ samples at 1050°C and 1100°C. It can be observed that grain coarsening occurs with sintering temperature increase and grain growth was seen with sintering temperature rise. XRD diffractograms of the sintered $Ni_{22}Cr_{11}Al$ at 1050°C and 1100°C were shown in Figures 6 and 7 along XRD results revealed diffraction peaks of all the elements . no phase transformation or decomposition is observed comparison with the starting powders.

The density values of the sintered $Ni_{22}Cr_{11}Al$ shows that the material is fully dense which indicates low porosity and voids. From
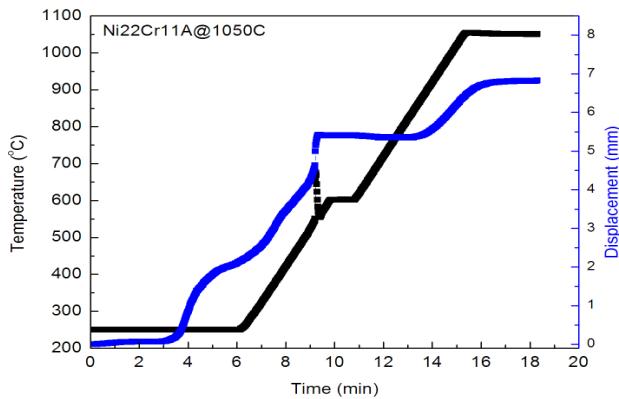
Figure 3b: The temperature and displacement curve in spark plasma sintering process at 1050°C.
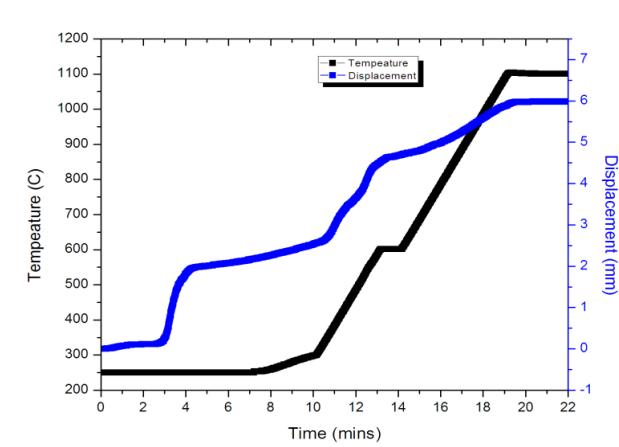

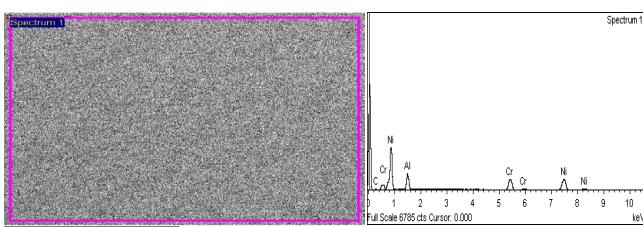**Figure 3c:** temperature and displacement curve in spark plasma sintering process at 1100°C.

Figure 4: SEM micrograph of Ni$_{22}$Cr$_{11}$Al powder (Left), EDS analysis (Right) sintered at 1050°C.

Figure 5: SEM micrograph of Ni$_{22}$Cr$_{11}$Al powder (Left), EDS analysis (Right) sintered at 1100°C.
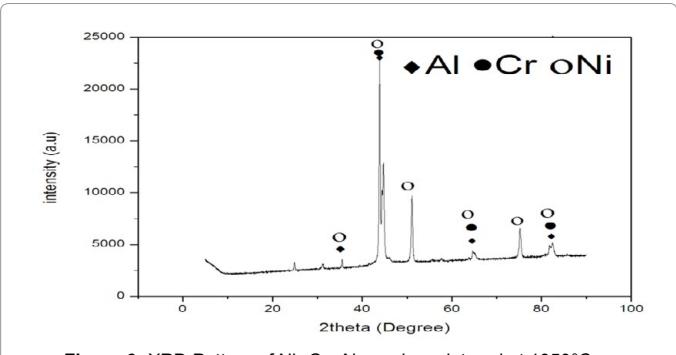
Figure 6: XRD Pattern of Ni$_{22}$Cr$_{11}$Al powders sintered at 1050°C.
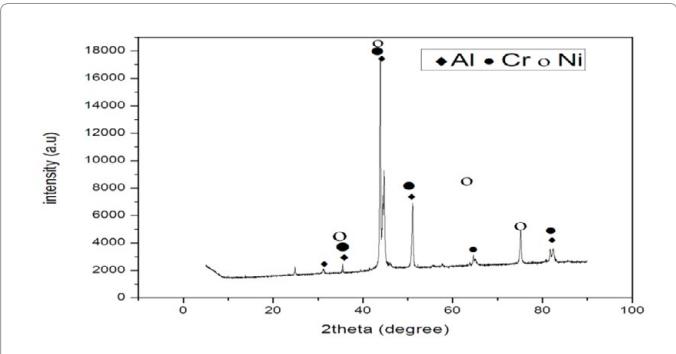
Figure 7: XRD pattern of Ni$_{22}$Cr$_{11}$Al powders sintered at 1100°C.

Powder (Ni$_{22}$Cr$_{11}$Al)	Sintering Temperatures	Relative Density
	1000°C	92.2
	1050°C	93
	1100°C	94

Table 2: Sintering temperature as compared with relative density.

Table 2 and Figure 8 where the relative density values increases with the sintering temperature because the grain size is getting higher at higher sintering temperature. The material may shrink slightly at higher sintering temperature ;therefore the density increase slightly. Density is mass per unit volume. Density of Ni = 8.908 g/cm³, Cr = 7.19 g/cm³, Al = 2.7 g/cm³. The density of the sintered grinded and polished bodies was determined by Archimedes principle using the density determination kit of OHAUS density scale. The Principle states that every solid body immersed in a fluid loss weight by an amount equal to that of the fluid it displaces.
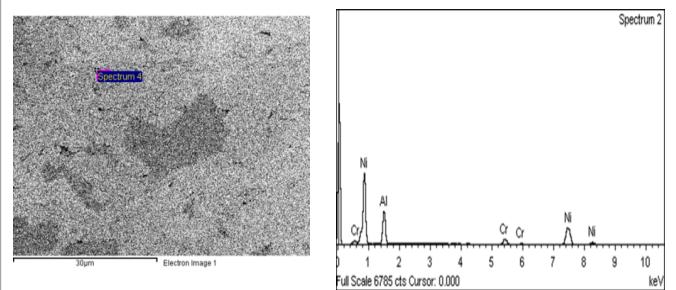
Density (Q) = A / (A-B) * Q0.

Where, A is weight of solid in air.

B is weight of solid in water.

Q0 is the density of water = 1.006 g/cm³

Micro hardness values of the sintered Ni$_{22}$Cr$_{11}$Al are shown in Table 3 and in Figure 9, hardness value increases with increasing sintering temperature from 1000°C to 1100°C, this is due to more developed sintering necks , rounder pores and change in microstructure. Consequently, the micrographs of the hardness was studied with SEM as shown in Figure 10, it was observed that extent of damages at the load 25 gf is governed by mechanism of intergranules and transgranular
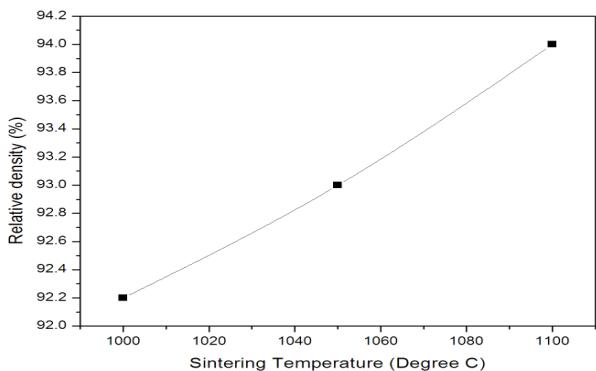
Figure 8: Effect of sintering temperature on relative density.

Powder Ni$_{22}$Cr$_{11}$Al	Sintering Temperatures	Av. Vickers Hardness 25gf
	1000°C	261.15
	1050°C	270.34
	1100°C	290.46

Table 3: Vickers micro hardness Hv at various sintering temperature.
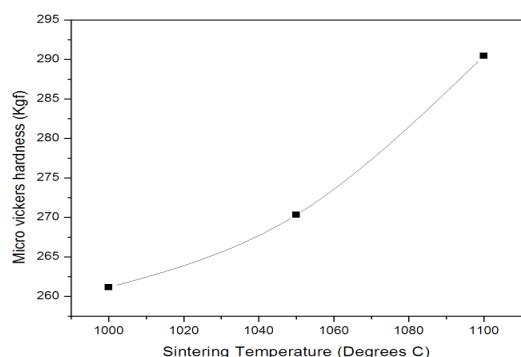
Figure 9: Vickers microhardness as a function of sintering temperature.

Figure 10: SEM micrographs of Vickers indents induced at different points.
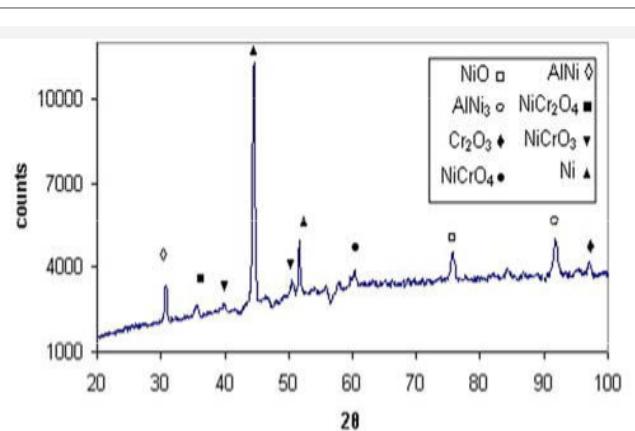
Figure 11: Micro XRD pattern after oxidation at 1100°C for 100h.

fracture, grain crushing and pulling effects.

Oxidation behaviour of sintered samples

NiCrAl alloy SPSed specimens were exposed for 20, 40, 100 hr at 1100°C.

SPSed: A thickness of 2-4 micro meters oxide layer is formed on the sample surface. According to the linear scan map, it is seen by EDS analysis that the layer is rich in Al as such corresponds to Al$_2$O$_3$ [22]. However, as reported in Figure 11, XRD analysis performed on the surface of oxidized samples reveals the presence of alumina and other oxides such as Cr$_2$O$_3$, spinel-like compounds like NiO, NiCr$_2$O$_4$ which are non-protective oxides [24-26]. It is well established that while the formation of slow-growing oxides alumina has to be maintained to prevent oxidation of the super alloy substrate, the presence of mixed oxides like spinels should be avoided as they grow too fast to produce protective scale [26-29].

When NiCrAl sintered samples are initially exposed to high temperature oxidizing environment, Al is the first element that tends to be preferentially oxidized [30-33]. From thermodynamic point of view Al has high affinity to react with 0$_2$, which brings about O$_2$ penetration and Al diffusion gives rise to Al$_2$O$_3$ formation [34-36]. EDS investigation

of the TGO reveals the high percentage of O$_2$ and Al and less of Cr and Ni element. Hence the main component of the TGO is Al$_2$O$_3$.

XRD patterns through the cross section of the bond coat after oxidation at 1100°C for 100 hr, revealed the oxides phases in the bond coat are NiCr$_2$O$_4$, NiCrO$_3$, NiCrO4, and NiO [37]. The degradation of the bondcoat leading to overall TBC failure is caused by these oxides formation accompanied with rapid volume increase [38,39].

Conclusion

Ni$_{22}$Cr$_{11}$Al powder sintered at 1000°C, 1050°C and 1100°C was produced. And the relative density of sintered sample was as high as 94%. Microstructure observation showed that the achieved coating was well dense with attractive mechanical properties at room temperature. The grain growth of the samples was seen with interesting sintering temperature. These features described above are attributed to the oxidation behaviour displayed by Ni$_{22}$Cr$_{11}$Al when exposed to air at high temperature. The homogeneity of the final sintered product coupled with microstructure refinement favour the selective formation of a continuous and dense layer of alumina while the presence of less protective mixed oxides (spinels) is hindered. SPS process indicates to be a promising technique due to shorter time process which gives rise to many advantages such as rapid turnover and low cost.

Reference

1. Chai Y, Chan P, Fu Y, Chang Y, Liu C (2008) Copper/Carbon nanotube composite interconnect for enhanced electromigration resistance. Electronic Components and Technology Conference, 2008, Lake Buena Vista, FL.

2. Bukhari MZ, Brabazon D, Hashmi MSJ (2011) Application of metal matrix composites cusic and alsic as electronics packaging materials. 28th International Manufacturing Conference.

3. Schubert T, Trindade B, Weißgärber T, Kieback B (2008) Interfacial design of cu-based composites prepared by powder metallurgy for heat sink applications. Mater Sci Eng A 475: 39-44.

4. Datsyuk V, Firkowska I, Gharagozloo-Hubmann K, Lisunova M, Vogt A, et al. (2011) Carbon nanotubes based engineering materials for thermal management applications. Semiconductor Thermal Measurement and Management Symposium (SEMI-THERM). 2011 27th Annual IEEE, San Jose, CA.

5. Cocke DL, Schennach R, Hossain MA, Mencer DE, McWhinney H, et al. (2005) The low-temperature thermal oxidation of copper, cu < sub > 3 < /sub > o < sub > 2 < /sub >, and its influence on past and future studies. Vacuum 79: 71-83.

6. Orth JE, Wheat HG (1997) Corrosion behavior of high energy-high rate consolidated graphite/copper metal matrix composites in chloride media. applied composite materials 4: 305-320.

7. Silvain JF, Vincent C, Heintz JM, Chandra N (2009) Novel processing and characterization of Cu/Cnf nanocomposite for high thermal conductivity applications. Composites Science and Technology 69: 2474-2484.

8. Sule R, Olubambi PA, Abe BT, Johnson OT (2012) Synthesis and characterization of sub-micron sized copper–ruthenium–tantalum composites for interconnection application. Microelectronics Reliability 52: 1690-1698.

9. Akbarpour MR, Salahi E, Alikhani Hesari F, Simchi A, Kim HS (2013) Fabrication, characterization and mechanical properties of hybrid composites of copper using the nanoparticulates of sic and carbon nanotubes. Materials Science and Engineering: A 572: 83-90.

10. O'reilly M, Jiang X, Beechinor JT, Lynch S, NiDheasuna C, et al. (1995) Investigation of the oxidation behaviour of thin film and bulk copper. Applied surface science 91: 152-156.

11. Deng CF, Ma YX, Zhang P, Zhang XX, Wang DZ (2008) Thermal expansion behaviors of aluminum composite reinforced with carbon nanotubes. Materials Letters 62: 2301-2303.

12. Thompson CV (2008) Carbon nanotubes as interconnects: Emerging technology and potential reliability issues. reliability physics symposium, 2008. IRPS 2008. IEEE International, Phoenix, AZ.

13. Nie J, Jia C, Jia X, Zhang Y, Shi N, et al. (2011) Fabrication, microstructures, and properties of copper matrix composites reinforced by molybdenum-coated carbon nanotubes. Rare Metals 30: 401-407.

14. Firkowska I, Boden A,Vogt AM, Reich S (2011) Effect of carbon nanotube surface modification on thermal properties of copper–cnt composites. Journal of Materials Chemistry 21: 17541-17546.

15. Damayantia M, Sritharan T, Mhaisalkar SG, Phoon E, Chan L (2007) Study of Ru Barrier failure in the Cu/Ru/Si system. J Mater Res Soc 22: 2505-2511.

16. Yang CC, Spooner T, Ponoth S, Chanda K, Simon A, et al. (2006) Physical, electrical, and reliability characterization of Ru for Cu interconnects. Interconnect Technology Conference, 2006 International, Burlingame, CA.

17. Wang Y, Cao F, Zhang ML, Liu YT (2011) Comparative study of Cu-Zr and Cu-Ru alloy films for barrier-free Cu metallization. Thin Solid Film 519: 3169-3172.

18. Ghosh D, Chen S (2008) Solid-state electronic conductivity of ruthenium nanoparticles passivated by metal-carbon covalent bonds. Chemical Physics Letters 465: 115-119.

19. Ding SF, Xie Q, Müeller S, Waechtler T, Lu HS, et al. (2011) The inhibition of enhanced Cu oxidation on ruthenium/diffusion barrier layers for Cu interconnects by carbon alloying into Ru. Journal of the Electrochemical Society 158: H1228-H1232.

20. Carreno-Morelli E, Yang J, Couter E, Hernadi K, Seo JW, et al. (2004) Carbon Nanotube/Magnesium Composites. Physical status solid 201: R53-R55.

21. Esawi A, Morsi K (2007) Dispersion of Carbon nanotubes (Cnts) in Aluminum powder. Composites Part A: Applied Science and Manufacturing 38: 646-650.

22. Yamanaka S, Gonda R, Kawasaki A, Sakamoto H, Mekuchi Y, et al. (2007) Fabrication and thermal properties of carbon nanotube/nickel composite by spark plasma sintering method. Materials Transactions 48: 2506-2512.

23. Kim C, Lim B, Kim B, Shim U, Oh S, et al. (2009) Strengthening of copper matrix composites by nickel-coated single-walled carbon nanotube reinforcements. Synthetic Metals 159: 424-429.

24. Cho S, Kikuchi K, Miyazaki T, Takagi K, Kawasaki A, et al. (2010) Multiwalled Carbon nanotubes as a contributing reinforcement phase for the improvement of thermal conductivity in copper matrix composites. Scripta Materialia 63: 375-378.

25. Bhat BN, Ellis D, Smelyanskiyv V, Foygel M, Rape A, et al. (2013) copper-multiwall carbon nanotubes and copper-diamond composites for advanced rocket engines.

26. Platzman I, Brener R, Haick H, Tannenbaum R (2008) Oxidation of Polycrystalline Copper Thin Films at Ambient Conditions. The Journal of Physical Chemistry C 112: 1101-1108.

27. Sule R, Olubambi PA, Sigalas I, Asante JKO, Garrett JC (2014) Effect of SPS consolidation parameters on submicron Cu and Cu–CNT composites for thermal management. Powder Technology 258: 198-205.

28. Hu Q, Luo P, Yan Y (2008) Influence of spark plasma sintering temperature on sintering behavior and microstructures of dense bulk mosi< sub> 2</sub>. Journal of Alloys and Compounds 459: 163-168.

29. Saheb N, Iqbal Z, Khalil A, Hakeem AS, Al-Aqeeli N, et al. (2012) Spark plasma sintering of metals and metal matrix nanocomposites: a review. Journal of Nanomaterials 2012: 18.

30. Pan MY, Gupta M, Tay AAO, Vaidyanathan K (2006) Development of bulk nanostructured copper with superior hardness for use as an interconnect material in electronic packaging. Microelectronics Reliability 46: 763-767.

31. Sule R, Olubambi PA, Sigalas I, Asante JKO, Garrett JC (2014) Densification and fracture characteristics of spark plasma sintered Copper- CNT- Ruthenium composites. Proceedings Euro PM2014 - PM for current and Future Applications (2014) Austria.

32. Xue ZW, Wang LD, Zhao PT, Xu SC, Qi JL, Fei WD (2012) Microstructures and tensile behavior of carbon nanotubes reinforced Cu matrix composites with molecular-level dispersion. Materials and Design 34: 298-301.

33. Gupta M, Tay AAO, Vaidyanathan K, Srivatsan TS (2007) An investigation of the synthesis and characterization of copper sample for use in interconnect application. Mater Sci A 454-455: 690-694.

34. Lee KM, Oh DK, Choi WS, Weissgärber T, Kieback B (2007) Thermomechanical properties of Aln-Cu composite materials prepared by solid state processing. Journal of Alloys and Compounds 434-435: 375-377.

35. Tong XC (2011) Advanced materials for thermal management of electronic packaging. Springer.

36. James JD, Spittle JA, Brown SGR, Evans RW (2001) A review of measurement techniques for the thermal expansion coefficient of metals and alloys at elevated temperatures. Measurement Science and Technology 12: R1.

37. Pollack GL (1969) Kapitza resistance. Review of modern physics 41: 48-81.

38. Chu K, Guo H, Jia C, Yin F, Zhang X, et al. (2010) Thermal properties of carbon nanotube-copper composites for thermal management applications. Nanoscale research letters 5: 868-874.

39. Wagner CD, Naumkin AV, Kraut-Vass A, Allison JW, Powell CJ, et al. (2003) X-Ray photoelectron spectroscopy database. Nist Standard Reference Database 20, Version 3.4.